

Self-consistent field theory for the distal ordering of adsorbed polymer: comparison with the Scheutjens–Fleer model

Karl Isak Skau, Edgar M. Blokhuis, and Jan van Male

Colloid and Interface Science, Leiden Institute of Chemistry,

Gorlaeus Laboratories, P.O. Box 9502, 2300 RA Leiden, the Netherlands.

September 14, 2018

Abstract. In a previous article [E.M. Blokhuis, K.I. Skau, and J.B. Avalos, *J. Chem. Phys.* **119**, 3483 (2003)], a self-consistent field formalism was derived for weakly adsorbing polymers, valid for any chain length. It was shown that the presence of a solid wall induces an ordering of the polymers on the scale of the radius of gyration far away from the surface (the distal region). These oscillations in the polymer concentration profile were first noted in work by Semenov *et al.*, and later observed in numerical solutions of the Scheutjens and Fleer self-consistent field model. In the present paper, we compare the weak adsorption model in more detail with the numerical results from the Scheutjens and Fleer model. Quantitative agreement is obtained for the polymer segment density profile in a good (athermal) solvent. For theta solvent and poor solvent conditions, it is necessary to extend the weak adsorption model to take the non-local character of the polymer–solvent interaction into account. Again, quantitative agreement is obtained for the polymer segment density profile, in particular for the transition from an oscillatory decaying profile to a monotonically decaying profile when the bulk polymer density is below a certain threshold value.

1 Introduction

The adsorption of polymer onto a solid surface has received considerable attention both from an experimental and a theoretical point of view. Interest in these systems is driven by practical applications, but also as a testing ground for various theoretical approaches [1–3].

Theoretically, surfaces with enhanced polymer adsorption were first studied by de Gennes [1,4] in the context of the Edwards self-consistent field theory [5]. In the de Gennes free energy functional, the so-called *ground state dominance approximation* [1,5,6] is made in which the polymer chain length is essentially set to infinity. Various extensions of the de Gennes model have been formulated. In work by de Gennes [4] and Rossi and Pincus [7] the correct scaling behavior was incorporated into the free energy functional, whereas Semenov and coworkers have extended the de Gennes model to determine finite chain length corrections [8–12]. The latter calculations are of particular interest since the polymer chain length is an important parameter in experiments [13] and computer simulations [14–16]. Variation of the chain length thus provides a more stringent testing of theoretical models [17].

A versatile model for the theoretical description of polymer adsorption is the Scheutjens and Fleer [18,19] self-consistent field model. The Scheutjens–Fleer model (SF) is a generalization of the Flory–Huggins mean-field lattice model [13] extended to describe inhomogeneous polymer systems. In the SF model, the Edwards [5] self-consistent field equations for the polymer’s Green function are solved numerically on a lattice. The capability and flexibility of the SF model has been demonstrated with its use to calculate properties of inhomogeneous polymer systems containing homopolymers, copolymers and polyelectrolytes and also surfactant systems like micelles and membranes [2]. In recent years, the SF algorithm has been made available in the multipurpose computer program SFBOX [20].

Recently, a self-consistent field formalism was derived for weakly adsorbed polymers, valid for any chain length [21]. One notable difference from the classical ground state dominance result of de Gennes [1] is the distal ordering of the polymers; the finite chain length gives rise to oscillations on the scale of the radius

of gyration away from the surface. These oscillations in the polymer concentration profile were first noted in work by Semenov *et al.* [8, 11], and later observed [22] in the numerical solutions of the Scheutjens and Fler self-consistent field model. The onset of these oscillations has also appeared in the context of analytical work and computer simulations [15, 21, 23].

In the present paper, we compare the free energy functional formalism for weak adsorption [21] with the numerical results from the Scheutjens and Fler model. In particular we address the observation made by van der Gucht *et al.* [22] that in a theta solvent, the oscillatory decaying function becomes a monotonically decaying function when the bulk polymer density is below a certain threshold value, similar to the Fisher–Widom transition [24, 25] in the damped oscillations found in a simple liquid near a surface. Our comparison will therefore consider some general properties of the distal ordering in both good and theta solvent conditions.

The outline of this article is as follows: In the next two sections we discuss the self-consistent field theory for weak adsorption, in the context of which our calculations are made, and the Scheutjens and Fler self-consistent field model. In Section 4, we make the comparison between our analytical results and numerical calculations carried out with the help of the computer program SFBOX. We end with a discussion of results.

2 Self-consistent field theory

The Green function $G(\mathbf{r}, \mathbf{r}', N)$ describes the statistical weight of a single polymer chain of length N with one end at \mathbf{r} and the other end at \mathbf{r}' . The Green function is determined by the Edwards equation [5]:

$$\frac{\partial}{\partial n} G(\mathbf{r}, \mathbf{r}', n) = \frac{a^2}{6} \nabla^2 G(\mathbf{r}, \mathbf{r}', n) - \frac{U(\mathbf{r})}{k_B T} G(\mathbf{r}, \mathbf{r}', n), \quad (2.1)$$

where a is the polymer segment length and $U(\mathbf{r})$ is an as yet unspecified external potential. As an initial condition to the Edwards equation, we have that

$$\lim_{n \rightarrow 0} G(\mathbf{r}, \mathbf{r}', n) = \delta(\mathbf{r} - \mathbf{r}'). \quad (2.2)$$

In terms of the Green function, one can construct the average segment density:

$$\phi(\mathbf{r}) = a^3 N_p \frac{\int_0^N dn \int d\mathbf{r}' \int d\mathbf{r}'' G(\mathbf{r}', \mathbf{r}, n) G(\mathbf{r}, \mathbf{r}'', N - n)}{\int d\mathbf{r}' \int d\mathbf{r}'' G(\mathbf{r}', \mathbf{r}'', N)}, \quad (2.3)$$

where N_p is the total number of polymer chains. This prefactor determines the scale of the Green function; it is chosen such that the density is equal to the given, uniform bulk density, $\phi(\mathbf{r}) = a^3 N_p N/V \equiv \phi_b$, for a homogeneous system. Here, $\phi(\mathbf{r})$ is the polymer segment *number* density made dimensionless by the factor a^3 and can thus be interpreted as the polymer segment *volume* fraction.

The statistical weight $G(\mathbf{r}, n)$ of a polymer chain with one end at position \mathbf{r} is obtained by integrating the Green function over one of the chain's ends:

$$G(\mathbf{r}, n) \equiv \int d\mathbf{r}' G(\mathbf{r}, \mathbf{r}', n). \quad (2.4)$$

For the case of polymer adsorption onto a planar, solid surface, the segment density profile and Green function only depend on the coordinate z so that $\phi(\mathbf{r}) = \phi(z)$ and $G(\mathbf{r}, n) = G(z, n)$. In the (isotropic) bulk region $G(z, n) \rightarrow G_b(n)$, i.e. independent of z . By solving the Edwards equation (2.1) with the initial condition in Eq.(2.2), one may show that in the bulk region: $G_b(n) = e^{-U_b n/k_B T}$, where we have defined $U_b \equiv U(z = \infty)$. It is convenient to redefine the statistical weight to absorb this trivial n -dependence:

$$Z(z, n) \equiv e^{U_b n/k_B T} G(z, n). \quad (2.5)$$

The Edwards equation (Eq.(2.1)) and segment density (Eq.(2.3)) are then given by

$$\frac{\partial}{\partial n} Z(z, n) = \frac{a^2}{6} \frac{\partial^2}{\partial z^2} Z(z, n) - \left[\frac{U(z) - U_b}{k_B T} \right] Z(z, n), \quad (2.6)$$

$$\phi(z) = \frac{\phi_b}{N} \int_0^N dn Z(z, n) Z(z, N - n), \quad (2.7)$$

with the initial condition:

$$\lim_{n \rightarrow 0} Z(z, n) = 1. \quad (2.8)$$

In the self-consistent field model, the external potential $U(z)$ is in turn expressed in terms of the polymer segment density with the result that the set of equations

(2.6)-(2.7) becomes self-consistently closed. Various forms for the self-consistent external potential in terms of the segment density may be proposed. It should in some way describe the interaction between different polymer segments and of the polymer segments with the solid wall. A convenient form would be:

$$\frac{U(z)}{k_{\text{B}}T} = v_0 \phi(z) + \frac{w_0^2}{2} \phi(z)^2 - m \phi''(z) + \frac{U_{\text{wall}}}{k_{\text{B}}T}, \quad (2.9)$$

The first two terms describe the polymer segment interaction in a virial expansion where v_0 , the so-called *excluded volume* parameter, is proportional to the second virial coefficient and w_0^2 is proportional to the third virial coefficient of segment-segment interactions. The third term describes the *non-local* character of the interaction and reflects the non-homogeneous nature of the polymer segment distribution. Such a term is analogous to the squared-gradient term in the van der Waals theory for the liquid-vapor interface. The last term in Eq.(2.9) gives the interaction with the wall. In the following we will assume that it is short-ranged and that it can be approximated by a delta function located *at* the wall [1]:

$$\frac{U_{\text{wall}}}{k_{\text{B}}T} = -\frac{a^2}{6} \frac{1}{d} \delta(z). \quad (2.10)$$

The parameter $d > 0$ is termed the extrapolation length [1]; its inverse is a measure of the surface interaction strength and leads to enhanced polymer adsorption, $\phi(0) > \phi_b$. In the following, we will investigate the situation where $1/d$ is small [21] leading to *weak adsorption*.

Weak adsorption

The assumption of weak polymer adsorption implies that $\delta\phi(z) \equiv \phi(z) - \phi_b \ll \phi_b$ and $\delta Z(z, n) \equiv Z(z, n) - 1 \ll 1$. Linearization of Eqs.(2.6) and (2.7) then leads to:

$$\frac{\partial}{\partial n} \delta Z(z, n) = \frac{a^2}{6} \frac{\partial^2}{\partial z^2} \delta Z(z, n) - \frac{\delta U(z)}{k_{\text{B}}T}, \quad (2.11)$$

$$\delta\phi(z) = \frac{2\phi_b}{N} \int_0^N dn \delta Z(z, n), \quad (2.12)$$

with the initial condition:

$$\lim_{n \rightarrow 0} \delta Z(z, n) = 0. \quad (2.13)$$

The general form for the external potential expanded around $\phi = \phi_b$ is given by

$$\frac{\delta U(z)}{k_{\text{B}}T} = v \delta\phi(z) - m \delta\phi''(z) - \frac{a^2}{6} \frac{1}{d} \delta(z). \quad (2.14)$$

The dimensionless parameter v is a *generalized excluded volume parameter*. Since we have expanded around $\phi = \phi_b$ rather than around $\phi = 0$, as is done in the virial expansion in Eq.(2.9), we have that $v = v(\phi_b)$ is not necessarily equal to the second virial coefficient ($v \neq v_0$) and thus may contain higher order interactions. For stability, we *do* require $v > 0$; to describe the situation $v < 0$, it would be necessary to include more terms in the expansion around ϕ_b . The above expression for the external potential is used when we make the comparison with the SF calculations.

For the situation that $m = 0$, it was shown [21] that the linearized set of equations in Eqs.(2.11)-(2.14) may be reformulated into a free energy functional formalism with the free energy functional given by

$$\begin{aligned} \frac{a^3 F[\delta\phi]}{A k_B T} &= \frac{1}{8 \phi_b N} \int_0^\infty dz \int_0^\infty dz' \delta\phi'(z) \delta\phi'(z') \left[\alpha_D\left(\frac{z-z'}{2R_g}\right) - \alpha_D\left(\frac{z+z'}{2R_g}\right) \right] \\ &+ \frac{v}{2} \int_0^\infty dz [\delta\phi(z)^2] - \frac{a^2}{6} \frac{1}{d} \phi(0). \end{aligned} \quad (2.15)$$

where the polymer's radius of gyration $R_g \equiv \sqrt{Na^2/6}$ and where

$$\alpha_D(x) \equiv \int_{-\infty}^{\infty} \frac{dk}{2\pi} e^{ikx} \frac{k^2}{k^2 - 4 + 4e^{-k^2/4}}. \quad (2.16)$$

Minimization of the free energy in Eq.(2.15) gives for the segment density profile [21]

$$\delta\phi(z) = \frac{\phi_b \xi_b^2}{\pi d R_g} \int_0^\infty dt \cos\left(\frac{tz}{R_g}\right) \left[\frac{t^2 - 1 + \exp(-t^2)}{(\varepsilon/4)t^4 + t^2 - 1 + \exp(-t^2)} \right], \quad (2.17)$$

where we have introduced the parameter ε as the (square of) the bulk correlation length, $\xi_b \equiv a/\sqrt{3v\phi_b}$, divided by the polymer's radius of gyration:

$$\varepsilon \equiv \frac{\xi_b^2}{R_g^2} = \frac{2}{v \phi_b N}. \quad (2.18)$$

The expression for the free energy can be generalized to the situation $m \neq 0$

$$\begin{aligned} \frac{a^3 F[\delta\phi]}{A k_B T} &= \frac{1}{8 \phi_b N} \int_0^\infty dz \int_0^\infty dz' \delta\phi'(z) \delta\phi'(z') \left[\alpha_D\left(\frac{z-z'}{2R_g}\right) - \alpha_D\left(\frac{z+z'}{2R_g}\right) \right] \\ &+ \frac{1}{2} \int_0^\infty dz [v \delta\phi(z)^2 + m \delta\phi'(z)^2] - \frac{a^2}{6} \frac{1}{d} \phi(0). \end{aligned} \quad (2.19)$$

The resulting segment density profile is then given by

$$\delta\phi(z) = \frac{\phi_b \xi_b^2}{\pi d R_g} \int_0^\infty dt \cos\left(\frac{tz}{R_g}\right) \left[\frac{t^2 - 1 + \exp(-t^2)}{(\varepsilon/4) t^4 + (1 + \beta t^2) (t^2 - 1 + \exp(-t^2))} \right], \quad (2.20)$$

where we have introduced the parameter β as the (square of) the length defined by the ratio of m and v , $\xi_m \equiv \sqrt{m/v}$, divided by the polymer's radius of gyration:

$$\beta \equiv \frac{\xi_m^2}{R_g^2} = \frac{6 m}{N a^2 v}. \quad (2.21)$$

The length ξ_m is the typical length scale connected to spatial inhomogeneities in the segment density caused by the interactions between segments excluding interactions due to the chain's connectivity (which are described by ξ_b). In a good solvent ξ_b dominates over ξ_m while ξ_m gains in significance near the theta region.

The main goal in this article is to compare the segment density profiles given in Eqs.(2.17) and (2.20) to numerical results from the Scheutjens and Fler lattice model.

3 Scheutjens and Fler self-consistent field model

The Scheutjens–Fler model [18,19] gives an efficient way to solve, self-consistently, the discrete version of the Edwards equation (2.6) on a lattice. The lattice distance is taken to be equal to the polymer segment length a , and $1/\lambda$ is the lattice coordination number that we set equal to $1/\lambda=6$ corresponding to a cubic lattice. The distance z away from the surface is here a discrete variable, $z = 0, 1, \dots, M$ layers (See Figure 1). A hard surface is located at $z = 0$, and at $z = M$ we have reflective boundary conditions (M should be chosen large enough for the system to reach bulk density).

The polymer is modeled as a one-dimensional walk perpendicular to the surface, where the walk can either move to the neighboring layer or stay in the layer it already is. Each step is weighted with the probability of going to a neighboring layer (λ) or staying in the same layer ($1 - 2\lambda$). This gives the following recurrence relation for the Green function $G(z, s)$ (the discrete analog of $Z(z, n)$), which is

the statistical weight of finding the end segment s of a chain in layer z ,

$$\begin{aligned} G(z, s+1) &= G(z) [\lambda G(z-1, s) + (1-2\lambda) G(z, s) + \lambda G(z+1, s)] , \\ &\equiv G(z) \langle G(z, s) \rangle . \end{aligned} \quad (3.1)$$

As a starting point for the recurrence relation we have that $G(z, 1) = G(z)$, the statistical weight of a single polymer segment. The brackets $\langle \dots \rangle$ denote the neighbor-weighted average as defined above. In the first layer, $z=1$, the neighbor-weighted average is defined as:

$$\langle G(1, s) \rangle \equiv (1-2\lambda) G(1, s) + \lambda G(2, s) . \quad (3.2)$$

In analogy with the continuous case, the segment density profile is obtained by summing over all possible paths of a polymer of length N passing through position z :

$$\phi(z) = \frac{\phi_b}{N} \sum_{s=1}^N \frac{G(z, s) G(z, N-s+1)}{G(z)} , \quad (3.3)$$

where the factor $G(z)$ in the denominator accounts for the double counting of the statistical weight at layer z . The statistical weight $G(z)$ is written as the Boltzmann factor of the segment potential

$$G(z) = e^{-U_{\text{SF}}(z)/k_{\text{B}}T} . \quad (3.4)$$

The segment potential $U_{\text{SF}}(z)$ accounts for the interactions between polymer segments and the surface-monomer interaction. The zero of the potential is at $z=\infty$ so that $U_{\text{SF}}(z=\infty) = 0$ and $G(z=\infty) = 1$. In the Scheutjens and Fler model the form for the segment potential is chosen such that it is consistent with the Flory–Huggins free energy expression for a homogeneous polymer solution [13]. It is given by [18]:

$$\frac{U_{\text{SF}}(z)}{k_{\text{B}}T} = -\ln \left(\frac{1-\phi(z)}{1-\phi_b} \right) - \chi (\langle \phi(z) \rangle - \langle 1-\phi(z) \rangle + 1 - 2\phi_b) - \chi_s \delta_{z,1} . \quad (3.5)$$

The first term is derived from the translational entropy of the “solvent molecules” (the sites not occupied by the polymer segments) in the Flory–Huggins theory. The second term describes the effective monomer–monomer interaction energy through the Flory parameter χ [13]. (Notice that this term is *non-local* since the

interactions between monomers in different layers is explicitly taken into account by the use of $\langle \phi(z) \rangle$ instead of $\phi(z)$.) The final term describes the surface-monomer interaction through the Silberberg parameter χ_s [26]. This parameter corresponds to the energy gain for a polymer segment to replace a solvent molecule at the surface ($z=1$).

As input parameters for the SF calculations we thus have: ϕ_b , N , χ , and χ_s . Many extensions to this model are possible and many have been made [2, 20]. One may, for example, introduce different polymer architectures, inhomogeneities in more than one dimension, and curved lattice geometries, but the underlying principles remain the same.

4 Comparison of results

To make a comparison between the density profiles from the analytical theory and the Scheutjens–Fleer self-consistent field model, one needs to relate the parameters in the analytical theory to those in the lattice model. In particular, one needs to: (i) relate the interaction parameters v and m to the Flory–Huggins parameter χ , and (ii) relate the extrapolation length d (or rather $1/d$) to the surface interaction parameter χ_s .

The discrete self-consistent field equations in the SF model can be transformed into continuous equations by assuming that the variations with z are small. In Appendix A we show that the recurrence relation in Eq.(3.1) then reduces to the continuous Edwards equation (2.6) with the external potential equal to $U_{\text{SF}}(z)$. To make the correspondence between χ and the parameters v and m , one therefore needs to expand the expression for $U_{\text{SF}}(z)$ in Eq.(3.5) around $\phi = \phi_b$, using that $\langle \phi \rangle \rightarrow \phi + (a^2/6) \phi''$ in the continuous limit (cf. Appendix A), and compare the result with $\delta U(z)$ in Eq.(2.14). One then finds that

$$v \longleftrightarrow \frac{1}{1 - \phi_b} - 2\chi, \quad m \longleftrightarrow \frac{a^2}{3} \chi. \quad (4.1)$$

It is less straightforward to arrive at a relation between the extrapolation length d and the surface interaction parameter χ_s . It should be realized that the presence of a solid surface is treated fundamentally different in the two models.

In the weak adsorption model, the treatment of the presence of the solid surface is derived from the de Gennes model for polymer adsorption [1]. In the de Gennes model, the free energy functional is strictly defined for $z > 0$; an interaction energy is added located at $z = 0$ (Eq.(2.10)), but such a term merely results in a boundary condition to the differential equation obtained from minimizing the free energy functional. As a result, the polymer segment density does not necessarily go to zero *at* the wall, $\phi(0) \neq 0$.

In the SF model, it is implicitly assumed that the polymer segment density at the wall is zero. This can be read off from the definition of the neighbor-weighted average in the first layer (see Eq.(3.2)), which for the segment density reads:

$$\langle \phi(1) \rangle = (1 - 2\lambda) \phi(1) + \lambda \phi(2), \quad (4.2)$$

i.e. $\phi(0) = 0$. It turns out that a consequence of this condition is that *enhanced* adsorption only occurs in the SF model above some threshold value, $\chi_s > \chi_{sc}$. The situation $\chi_s = \chi_{sc}$ then corresponds to the condition $1/d = 0$, which gives $\phi(z) = \phi_b$ for all z in the de Gennes model. The threshold value as a function of χ may therefore be determined by using that at the threshold one should have $\phi(z) \approx \phi_b$ for all z . For very long chains one finds: $\chi_{sc} = -\lambda \chi - \ln(1 - \lambda)$ [27]. Next, by comparing the expressions for the wall interaction terms in the two models, Eqs.(2.14) and (3.5), one arrives at the following identification [9, 27]

$$\frac{a^2}{6} \frac{1}{d} \delta(z) \longleftrightarrow (\chi_s - \chi_{sc}) \delta_{z,1} \quad \implies \quad \frac{a}{d} = 5 \left[\chi_s + \frac{\lambda}{6} - \ln(6/5) \right], \quad (4.3)$$

where we used that $\delta_{z,1} \longleftrightarrow a(1 - \lambda) \delta(z)$ [27].

We now have the necessary ingredients to compare the analytic expressions for the segment density profiles in Eqs.(2.17) and (2.20) to the numerical results of the SF model. It is good to realize that the inverse of the extrapolation length, $1/d$, only shows up as a prefactor to the analytic expressions for the segment density profile. Therefore, if one is interested in only the *qualitative* features of the segment density profile, knowledge of the precise value of $1/d$ is not needed. Only when one wants to make a quantitative comparison with the SF model, it is necessary to use the above relation between $1/d$ and χ_s .

Next, we first consider the case of an *athermal* solvent ($\chi = 0$) and compare the SF model results to Eq.(2.17). In particular, we will investigate the distal

oscillations for weak and strong polymer adsorption. Second, we consider a theta solvent ($\chi=1/2$), as was previously done by van der Gucht *et al.* [22], who showed that when the bulk density is below some threshold value, the oscillations in the distal profile disappear similar to the Fisher–Widom transition [24, 25] in the damped oscillations for a simple liquid near a surface. A quantitative comparison is made with the analytical expression for the segment density profile in Eq.(2.20). Finally, we consider the location of the Fisher–Widom transition with respect to the complete Flory–Huggins phase diagram [13] and also make a comparison with MC simulations [15].

4.1 Athermal solvent

For an *athermal* solvent we have that $\chi=0$ so that:

$$v = \frac{1}{1 - \phi_b} \approx 1, \quad m = 0. \quad (4.4)$$

In Figure 2a, the polymer segment density profile as calculated by the SF model is shown for two polymer chain lengths ($N=1000$ and $N=10000$) in the case of weak polymer adsorption ($\chi_s = 0.20$). To show $\delta\phi(z)/\phi_b$ on a logarithmic scale, here, and in later plots, the absolute value has been taken. Also shown as the solid line is the ground state dominance segment density profile [1]:

$$\phi(z) = \frac{\phi_b}{\tanh^2(z/\xi_b + x_0)}, \quad (4.5)$$

with the integration constant $x_0 = (1/2) \operatorname{arcsinh}(2d/\xi_b)$. In the comparison of Figure 2a, the expression for a/d in Eq.(4.3) was used.

The profiles corresponding to the two chain lengths are close to each other and close to the ground state dominance profile in this distance range. At very large distances, however, markedly different behavior can be observed; in Figure 2b, the same SF model results as in Figure 2a are plotted, showing oscillations in the segment density profile on the order of the polymer’s radius of gyration. The two solid lines in Figure 2b are the density profiles calculated by Eq.(2.17), using Eq.(4.3). Without any adjustable parameters, a strikingly good quantitative agreement between the SF model and Eq.(2.17) is obtained.

Even for strong adsorption the density profile in Eq.(2.17) is expected to give an accurate description for distances far away from the surface, since also there we have that $\delta\phi(z) \ll \phi_b$. However, since the density profile differs at short distances, the boundary condition may need to be replaced by some *effective* boundary condition. The result is that although the *shape* of the density profile is correctly described by Eq.(2.17) for strong adsorption, it may need to be shifted in the z -direction introducing the shift as an additional fit parameter. In Figure 3, the polymer segment density profile as calculated by the SF model is shown for a long polymer chain ($N=1000$) and for two values of the surface interaction parameter, $\chi_s = 0.25$ and $\chi_s = 1$, corresponding to strong adsorption. The solid lines are the density profiles calculated by Eq.(2.17), using Eq.(4.3) to set the scale of the y -axis. Furthermore, the density profiles are shifted in the z -direction by $-1.5 a$ (lower solid line) and $-4.5 a$ (top solid line). The asymptotic profiles are seen to indeed match quite well.

4.2 Theta solvent

We next consider the case of a Θ -solvent ($\chi=1/2$) where we have that

$$v = \frac{1}{1 - \phi_b} - 1 \approx \phi_b, \quad m = \frac{a^2}{6}. \quad (4.6)$$

It is good to realize that theta solvent conditions do not correspond to a vanishing generalized excluded volume parameter ($v \neq 0$).

In Ref. [22] the observation was made that the oscillations, prominently present in Figures 2 and 3, disappear in a Θ -solvent when the density is below a certain threshold bulk density, similar to the Fisher–Widom transition [24] for a simple liquid. In Figure 4, we show the characteristic signature of the Fisher–Widom (FW) transition going from $\phi_b = 0.01$ (solid line) to $\phi_b = 0.001$ (dashed line), for $N = 1000$ and for the same surface interaction strength, $\chi_s = -1/12$, as in Ref. [22]. (Note that this value is below the adsorption threshold value, so that we are dealing with polymer depletion instead of adsorption.) To understand this qualitative change in the behavior of the segment density profile, we further investigate the expression for the density profile in Eq.(2.20).

In Appendix B, it is shown that the asymptotic behavior is determined by the poles in the complex plane of the integrand's denominator of the expression for the density profile in Eq.(2.20). The resulting expression for the asymptotic segment density profile as given by Eq.(B.6) shows that the relevant poles correspond to either a purely exponentially decaying function:

$$\delta\phi(z) \propto \exp\left(-\frac{A_0 z}{R_g}\right), \quad (4.7)$$

or to an exponentially decaying sinusoid:

$$\delta\phi(z) \propto \exp\left(-\frac{A_1 z}{R_g}\right) \sin\left(\frac{B_1 z}{R_g} + \varphi\right). \quad (4.8)$$

Which of these two functions dominates the asymptotic behavior depends on the relative magnitudes of A_0 and A_1 ; when $A_0 > A_1$, the segment density decays asymptotically as an exponentially decaying sinusoid whereas it decays exponentially when $A_0 < A_1$. The value of the coefficients A_0 , A_1 and B_1 , depend on the value of the parameters ε and β . In Figure 5a, we have set $\beta = 0.18$ and plotted A_0 , A_1 and B_1 as a function of ε . At a certain value of ε (in this example: $\varepsilon^{\text{FW}} \approx 6.464$), A_0 and A_1 cross marking the location of the Fisher–Widom transition (arrow). By varying β , the whole locus of Fisher–Widom transitions can then be traced in this way (see Figure 5b).

To compare the analytically determined Fisher–Widom transition in Figure 5b with the results from the SF model, we located the Fisher–Widom transition by determining the bulk density where the *first* oscillation in the numerical density profiles disappears. This is the point where the first minimum (located closest to the wall) of the oscillating density profile crosses the value of the bulk density. This procedure gives only an approximation to the location of the real Fisher–Widom transition. A closer investigation reveals that the density oscillations do not disappear all at once at the same polymer bulk density; the first oscillation disappears before the second oscillation with decreasing bulk density, and presumably before all oscillations beyond that. Still, since the bulk densities at which subsequent oscillations vanish differ only slightly, we believe this procedure to give a fairly accurate approximation.

In Figure 6, the polymer segment density profile is shown for a Θ -solvent with $N = 10000$ for various bulk densities just below and above the Fisher–Widom

transition: $\phi_b = 0.00078$ (solid line), $\phi_b = 0.00082$ (dashed line), $\phi_b = 0.00086$ (dot-dashed line), and $\phi_b = 0.00090$ (dotted line). In (a), the density profiles are calculated in the SF model; in (b) the density profile is calculated using Eq.(B.6). Good quantitative agreement is obtained.

In Figure 7, we have located the Fisher–Widom transition in the SF model by determining the bulk density where the first oscillation disappears for different chain lengths (circles). The surface interaction strength $\chi_s = -1/12$, as in Ref. [22]. The numerical data are consistent with a scaling of the bulk density $\phi_b^* \sim 1/N$. The solid line is the Fisher–Widom transition shown in Figure 5b, where we have used that $N = \varepsilon/(2\beta^2)$ and $\phi_b = 2\beta/\varepsilon$ to transform from (ε, β) to (N, ϕ_b) as variables. Good agreement is obtained with the SF calculations.

Also shown in Figure 7, as the squares, are the SF calculations results for $N = 200$ and $N = 1000$ reported in Ref. [22], which differ somewhat from our results. Since these SF calculations are done with exactly the same set of parameters used to determine our results represented by circles, this difference must be attributed to the different procedure used in Ref. [22] to locate the Fisher–Widom transition. In the analysis in Ref. [22] the segment density profile is taken to be of the following form:

$$\frac{\delta\phi(z)}{\phi_b} = \tanh^2\left(\frac{z - z_0}{\xi_{b,\text{num}}}\right) - 1 + C_{\text{num}} \exp\left(-\frac{A_{\text{num}} z}{R_g}\right) \sin\left(\frac{B_{\text{num}} z}{R_g} + \varphi_{\text{num}}\right). \quad (4.9)$$

Then, by locating, as a function of ϕ_b , the position where $\xi_{b,\text{num}}/2$ equals R_g/A_{num} , the Fisher–Widom transition is determined.

Even though the analysis in Ref. [22] is done in a more judicious manner than simply fitting the numerical segment density profile to Eq.(4.9) (see Ref. [22] for details), the large number of parameters involved makes it difficult to accurately determine the location of the Fisher–Widom transition—especially since at the transition the relevant length scales cross. For instance, in the example shown in Figure 4, the Fisher–Widom transition as determined by the bulk density where the first oscillation disappears, is located at $\phi_b^{\text{FW}} \approx 0.00707$, whereas the value reported in Ref. [22] is $\phi_b^{\text{FW}} \approx 0.032$. This result would imply that the density profile depicted by the solid line in Figure 4 for $\phi_b = 0.01$ lies in the purely exponentially decaying-region, which seems unlikely.

Nevertheless, it is expected that this fitting procedure is more reliable in the region where the different length scales are well-separated, e.g. when $\phi_b \gg \phi_b^{\text{FW}}$. In this region, the fit parameters were numerically determined as [22]

$$A_{\text{num}} \simeq \frac{1}{0.19 \sqrt{6}} \simeq 2.1, \quad B_{\text{num}} \simeq \frac{2\pi}{1.5 \sqrt{6}} \simeq 1.7, \quad \xi_{b,\text{num}} \simeq \frac{0.52 a}{\phi_b}. \quad (4.10)$$

These values can be compared to the analytical density profile in the corresponding regime: $\varepsilon \ll 1$ and $\beta \ll 1$. For $\beta = 0$ and expanding in ε , it was shown that the segment density profile is then given by [21]

$$\frac{\delta\phi(z)}{\phi_b} = \frac{\xi_b}{d} e^{-2z/\xi_b} + C \exp\left(-\frac{Az}{R_g}\right) \sin\left(\frac{Bz}{R_g} + \varphi\right), \quad (4.11)$$

with

$$A = 2.217792\dots, \quad B = 1.682188\dots, \quad \xi_b = \frac{1}{\sqrt{3}\phi_b} \simeq \frac{0.58 a}{\phi_b}. \quad (4.12)$$

Thus, we find in the region $\phi_b \gg \phi_b^{\text{FW}}$ good agreement between the analytical results [21] and the fitting parameters in Eq.(4.10).

4.3 Phase diagram

Since the Fisher–Widom transition found in a Θ -solvent seems to be absent in an athermal solvent, it is worthwhile to locate the Fisher–Widom transition as a function of solvent quality.

In Figure 8, the Fisher–Widom transition is shown with respect to the full polymer phase diagram for $N = 100$. As a reference, the Flory–Huggins spinodal and binodal regions (dashed lines) are also shown [13]. The symbols are the SF results for the Fisher–Widom transition for enhanced polymer adsorption $\chi_s = 0.5$ (circles) and for polymer depletion $\chi_s = 0$ (squares). The solid line is the Fisher–Widom transition plotted in Figure 5b transformed from (ε, β) to (χ, ϕ_b) as variables, using Eq.(4.1). Good agreement is obtained with the SF calculations, independent of the polymer-wall interaction strength.

In the derivation of the analytical result for the Fisher–Widom transition, we have assumed that the generalized excluded volume parameter is always positive, $v > 0$. To verify that the Fisher–Widom transition lies within the region of applicability, the locus of points where $v = 0$ (which gives $2\chi = 1/(1 - \phi_b)$) is shown in

Figure 8 as the dotted line. Furthermore, the approximate location of the dilute to semi-dilute transition ($\phi^* = 1/(vN)$ [28], with v given by Eq.(4.1)) is shown as the dot-dashed line in Figure 8. Since both the mean-field model presented here as well as the SF model are expected to be reliable only in semi-dilute and concentrated solutions, the location of the Fisher–Widom transition shown is physically most relevant in the theta region.

As a final remark, we mention that a useful approximation to the location of the Fisher–Widom transition can be obtained by approximating β^{FW} by its $\varepsilon \rightarrow 0$ value: $\beta^{\text{FW}} \approx 0.20$ (see Figure 5b). This gives $2\chi^{\text{FW}} \approx N/[(N+5)(1-\phi_b)]$. For very long polymer chains, the Fisher–Widom transition thus approaches the line where $v=0$.

4.4 Comparison with Monte Carlo simulations

Recently, de Joannis *et al.* [15] performed Monte Carlo (MC) simulations of polymer chains at surfaces in an athermal solvent. In Figure 9a, the reduced segment density $\delta\phi(z)/\phi_b$ is shown as a function of z/R_g (Figure 9b shows the same profiles on a logarithmic scale). For the MC simulations (circles), the following parameter values were used: chain length $N=200$, bulk density $\phi_b=0.0216$, radius of gyration $R_g/a=9.76$, and surface interaction strength $\varepsilon_s = 1.0 k_B T$ [15]. The squares are the results from the SF model for the same parameters ($N=200$, $\chi=0$, bulk density $\phi_b=0.0216$) taking $\chi_s=1.0$ (variation of χ_s does not lead to very different results). Shown as the solid and dashed line is the density profile calculated using Eq.(2.17) for $a/d=7.35$ and $a/d=4.09$, respectively (both profiles are shifted in the z -direction to fit the data). The value of $a/d=7.35$ was chosen such that the depth of the minimum in the segment density profile matches that of the MC simulations, whereas the value of $a/d=4.09$ was chosen to correspond to $\chi_s=1.0$ (using Eq.(4.3)). The SF model corresponds well with the MC results although the depth of the minimum differs by a factor of two. The asymptotic formula in Eq.(2.17) is able to describe the MC-data (two fitting parameters) and SF model (one fitting parameter) well. So, also in the Monte Carlo simulations oscillations in the polymer concentration profile can be observed, even though it is not pos-

sible from the numerical data (and it is hard to get more accurate profiles) to observe more than the first oscillation.

5 Discussion

In this article, we have compared the analytic expressions for the segment density profiles obtained in the context of the weak adsorption model [21] to the numerical results of the Scheutjens–Fleer model [18, 19]. The analytic expressions are expected to be valid when the polymer adsorbs only weakly to the solid surface or, for strong adsorption, when the distance to the surface is large. Indeed, excellent quantitative agreement for the distal, oscillatory density profile was obtained for very good (athermal) solvent conditions, for both weak and strong polymer adsorption (Figures 2 and 3).

We have further investigated the previously observed Fisher–Widom transition in SF model calculations by van der Gucht *et al.* [22] for a Θ -solvent. We demonstrated that the location of the Fisher–Widom transition can be described by the weak adsorption model when the non-local character of the monomer–solvent interaction is taken into account. The quantitative agreement that is then achieved (see Figures 6, 7 and 8), gives confidence in identifying the non-local character of the interactions in the SF model as the source of the Fisher–Widom transition observed [22]. To further substantiate this identification, we also carried out separate SF calculations in which the non-local interactions were removed by replacing $\langle \phi(z) \rangle$ by $\phi(z)$ in Eq.(3.5). In this way, we could explicitly verify [29] that without the non-local interactions present, the oscillations always remain with decreasing bulk polymer concentration while maintaining the quantitative agreement with the segment density profiles of the weak adsorption model.

Although it is shown that the introduction of a non-local interaction term is useful for the comparison with the SF model, one should address the relevance of it when comparing with real, experimental polymer systems. Both the model presented here as well as the SF model are based on the mean-field assumption which is expected to be reasonable for semi-dilute and concentrated solutions (overlapping polymer coils) but is expected to fail for dilute solutions (isolated

coils), where fluctuations and inhomogeneities are more pronounced. Under good solvent conditions the Fisher–Widom transition occurs at polymer concentrations well below the dilute to semi-dilute transition, $\phi_b^{\text{FW}} \ll \phi^* \sim 1/(v_0 N)$ [28], and the mean-field results for the location of the Fisher–Widom transition are probably not so reliable. In theta and poor solvent conditions, close to the spinodal decomposition region (theta region), the Fisher–Widom transition shifts to much larger concentrations and occurs at a concentration comparable to the dilute to semi-dilute transition concentration, $\phi_b^{\text{FW}} \simeq \phi^* \sim 1/(w_0 N^{1/2})$ [28] (see Figure 8). We therefore expect our mean-field results to be most relevant to describe the occurrence and location of the Fisher–Widom transition in experimental polymer systems in the theta region.

It may seem somewhat surprising that the non-local interactions in the SF model, whose range is only one lattice distance a , may interfere with the oscillatory behavior on the scale of the polymer’s radius of gyration. However, the length scale connected with the non-local character is rather $\xi_m \equiv \sqrt{m/v}$ which diverges (similar to the bulk correlation length near the critical point in an ordinary liquid) when v is small, i.e. when the solvent is poor enough.

The Fisher–Widom transition in a simple liquid occurs when the attractive part of the interaction potential between the molecules dominates over the repulsive part [24, 25]. For high densities the hard core interaction gives damped oscillations away from the surface, while these oscillations disappear when the inter-molecular attraction balances the repulsion. The similarity with the transition observed for polymers is striking; the Θ -point defines the system conditions where the monomer attraction cancels the monomer repulsion. For a good solvent the effective monomer interaction is repulsive and oscillations are predicted for all densities [21]. There are, however, nontrivial differences between monomers and liquid molecules; the most important difference, of course, is the polymer chain connectivity. The chain connectivity gives rise to oscillations with a wavelength of the size of polymer coil, while in a simple liquid the wavelength is given by the molecular radius. It is tempting to think of the polymer solution as a “liquid” of polymer coils close to the surface. But this intuitive idea fails to consider the strong interdigitation of the coils at semi-dilute concentrations and that the coil

changes its conformation and size close to the surface (while a liquid molecule keeps its hard core shape). One should therefore be careful to make too much out of such analogies.

In the comparison of the Scheutjens and Flerer model [18, 19] to analytical theories such as the de Gennes model [1, 4], and extensions thereof such as the weak adsorption model [21], a number of differences can be distinguished. A clear difference is the fact that the SF model is a lattice model with the obvious consequence that the parameter describing the distance to the substrate is discrete; $z = 1, 2, 3, \dots$. The discreteness of space is most consequential in the very vicinity of the wall, where the monomer length scale becomes important.

Another important difference between the SF model and the de Gennes-like models concerns the boundary condition at the wall. In these latter models, the free energy functional is only strictly defined for $z > 0$. An interaction energy is defined located at $z = 0$, but the addition of such a term merely serves as a boundary condition to the differential equation which results from the minimization of the free energy functional. The result is that the polymer segment density not necessarily goes to zero *at* the wall, $\phi(0) \neq 0$. Even though in real polymer systems, the polymer segment density should become zero (or exponentially close to it) at some point, it is expected that a microscopic shift in the precise location of the wall—this location is not well-defined within a microscopic distance anyway—should restore the validity of the de Gennes-like models at least for enhanced polymer adsorption [4].

In the SF model, the free energy functional is already defined for whole space from the start. The reason that the density profile is zero when $z \leq 0$ is due to the explicit addition of an external potential which gives an infinite energy penalty for $z \leq 0$. Apart from this external potential there may be an energy contribution to the first layer at $z = 1$ which will generally be attractive. The result of the infinite repulsion at $z \leq 0$ is that the polymer density is zero at the wall $\phi(0) = 0$. The presence of this extra boundary condition makes the SF model essentially different from the de Gennes-like models, but similar to the single chain mean-field theory by Szleifer and others [30, 31] and computer simulations [14–16]. This boundary condition (but without the presence of any additional attraction) is also used in

the calculations by Eisenriegler and coworkers [3, 32, 33]. Still, it seems, as we have done here, that a meaningful comparison between the SF model and the de Gennes-like models can still be made when the adsorption energy in the first layer is above some given threshold value.

A Discrete and continuous Edwards equation

In this appendix, we show [2] how the recurrence relation for $G(z, s)$ in Eq.(3.1) in continuous form reduces to the Edwards equation (2.6). First, we rewrite the recurrence relation for $G(z, s)$ as:

$$G(z, s + 1) e^{U_{\text{SF}}(z)/k_{\text{B}}T} = G(z, s) + \lambda [G(z - 1, s) - 2G(z, s) + G(z + 1, s)] , \quad (\text{A.1})$$

where we used the expression for $G(z)$ in Eq.(3.4). To go from the discrete description to the continuous one, we assume that $G(z, s)$ is a slowly varying function of z and s . This means that:

$$G(z, s + 1) = G(z, s) + \frac{\partial}{\partial s} G(z, s) + \dots , \quad (\text{A.2})$$

and, keeping in mind that the distance z was rescaled by a , that

$$G(z \pm 1, s) \longrightarrow G(z \pm a, s) = G(z, s) \pm a \frac{\partial}{\partial z} G(z, s) + \frac{a^2}{2} \frac{\partial^2}{\partial z^2} G(z, s) + \dots . \quad (\text{A.3})$$

When $G(z, s)$ is a slowly varying function, it implies that the potential $U_{\text{SF}}(z)$ is close to its asymptotic value $U_{\text{SF}}(z \rightarrow \infty) = 0$, so that we can expand

$$e^{U_{\text{SF}}(z)/k_{\text{B}}T} \approx 1 + \frac{U_{\text{SF}}(z)}{k_{\text{B}}T} . \quad (\text{A.4})$$

Combining Eqs.(A.2)-(A.4) with Eq.(A.1) then gives:

$$\frac{\partial}{\partial s} G(z, s) = \lambda a^2 \frac{\partial^2}{\partial z^2} G(z, s) - \frac{U_{\text{SF}}(z)}{k_{\text{B}}T} G(z, s) , \quad (\text{A.5})$$

which, for $\lambda = 1/6$, is the Edwards equation in Eq.(2.6).

B Asymptotic behavior of the density profile

In this appendix, we investigate the asymptotic behavior of the polymer segment density profile given in Eq.(2.20). We write Eq.(2.20) as:

$$\delta\phi(z) = \frac{\phi_b \xi_b^2}{\pi d R_g} \int_0^\infty dt \cos(xt) Q(t), \quad (\text{B.1})$$

where we have defined $x \equiv z/R_G$ and $Q(t) \equiv f(t)/g(t)$ with

$$\begin{aligned} f(t) &\equiv t^2 - 1 + e^{-t^2}, \\ g(t) &\equiv \frac{\varepsilon t^4}{4} + (1 + \beta t^2) (t^2 - 1 + e^{-t^2}). \end{aligned} \quad (\text{B.2})$$

The integral in Eq.(B.1) can be solved [34]

$$\int_0^\infty dt \cos(xt) Q(t) = \pi i \sum R', \quad (\text{B.3})$$

where

$$\sum R' \equiv \text{sum of residues of } Q(z) e^{ixz} \text{ in the upper half plane.}$$

The poles are determined by the zero's of $g(z)$ in the complex plane (see also [25]). It turns out that there are an infinite number of poles in the upper half plane. Luckily, to describe the asymptotic behavior of Eq.(B.1), it is sufficient to locate the pole with the lowest imaginary part. Depending on the value of ε and β , this pole is either purely imaginary—let's denote it as $z_0 = iA_0$ —or it is complex and then it comes in pairs: $z_1 = \pm B_1 + iA_1$, where A_0 , A_1 , and B_1 are positive, real numbers. Taking only these three competing poles into account, we can determine the residues with the result:

$$\sum R' = i C_0 e^{-A_0 x} + 2i C_1 e^{-A_1 x} \sin(B_1 x + \varphi) + \dots, \quad (\text{B.4})$$

where

$$C_0 = \frac{f(z_0)}{g'(z_0)}, \quad C_1 = \left| \frac{f(z_1)}{g'(z_1)} \right|, \quad \varphi = \arg \left(\frac{f(z_1)}{g'(z_1)} \right), \quad (\text{B.5})$$

and where z_1 is taken to be the pole in the upper right quadrant.

As a final result, we thus have for the asymptotic density profile:

$$\delta\phi(z) = -\frac{2 \phi_b \xi_b^2}{d R_g} \left[\frac{C_0}{2} \exp\left(-\frac{A_0 z}{R_g}\right) + C_1 \exp\left(-\frac{A_1 z}{R_g}\right) \sin\left(\frac{B_1 z}{R_g} + \varphi\right) \right]. \quad (\text{B.6})$$

Acknowledgments

Without the continued help and interest of Josep Bonet Avalos, this work would not have been possible. The insightful comments of Albert Johner are, as always, very much appreciated.

References

- [1] de Gennes, P.G. *Scaling Concepts in Polymer Physics*; Cornell University Press: Ithaca, 1979.
- [2] Fler, G.J.; Cohen-Stuart, M.A.; Scheutjens, J.M.H.M.; Cosgrove, T.; Vincent, B. *Polymers at Interfaces*; Elsevier: London, 1993.
- [3] Eisenriegler, E. *Polymers near Interfaces*; World Scientific: Singapore, 1993.
- [4] de Gennes, P.G. *Macromolecules* **1981**, *14*, 1637. de Gennes, P.G. *Macromolecules* **1982**, *15*, 492.
- [5] Edwards, S.F. *Proc. Phys. Soc.* **1965**, *85*, 613. Edwards, S.F. *Proc. Phys. Soc.* **1966**, *88*, 265.
- [6] Lifshitz, I.M. *Soviet Phys. JETP* **1969**, *28*, 1280. Lifshitz, I.M.; Grosberg, A.Yu.; Khoklov, A.R. *Rev. Mod. Phys.* **1978**, *50*, 684.
- [7] Rossi, G.; Pincus, P.A. *Europhys. Lett.* **1988**, *5*, 641.
- [8] Semenov, A.N.; Bonet Avalos, J.; Johner, A.; Joanny, J.-F. *Macromolecules* **1996**, *29*, 2179.
- [9] Johner, A.; Bonet Avalos, J.; van der Linden, C.C.; Semenov, A.N.; Joanny, J.-F. *Macromolecules* **1996**, *29*, 3629.
- [10] Bonet Avalos, J.; Joanny, J.-F.; Johner, A.; Semenov, A.N. *Europhys. Lett.* **1996**, *35*, 97. Semenov, A.N.; Joanny, J.-F.; Johner, A.; Bonet Avalos, J. *Macromolecules* **1997**, *30*, 1479.
- [11] Semenov, A.N. *J. Phys. II* **1996**, *6*, 1759.

- [12] Semenov, A.N.; Joanny, J.-F.; Johner, A. *Polymer Adsorption: mean-field theory and ground state dominance approximation* in: “Theoretical and Mathematical Models in Polymer Research”. Grosberg, A., Ed.; Academic Press: San Diego, 1998.
- [13] Flory, P.F. *Principles of Polymer Chemistry*; Cornell University Press: Ithaca, 1953.
- [14] Binder, K. *Monte Carlo and Molecular Simulations in Polymer Sciences*; Oxford University Press: Oxford, 1995.
- [15] de Joannis, J.; Park, C.-W.; Thomatos, J.; Bitsanis, I.A. *Langmuir* **2001**, *17*, 69. de Joannis, J.; Ballamudi, R.K.; Park, C.-W.; Thomatos, J.; Bitsanis, I.A. *Europhys. Lett.* **2001**, *56*, 200.
- [16] Jiminez, J.; de Joannis, J.; Bitsanis, I.A.; Rajagopalan, R. *Macromolecules* **2000**, *33*, 7157. Jiminez, J.; de Joannis, J.; Bitsanis, I.A.; Rajagopalan, R. *Macromolecules* **2000**, *33*, 8512.
- [17] Skau, K.I.; Blokhuis, E.M. *Macromolecules* **2003**, *36*, 4637.
- [18] Scheutjens, J.M.H.M.; Fleer, G.J. *J. Phys. Chem.* **1979**, *83*, 1619. Scheutjens, J.M.H.M.; Fleer, G.J. *J. Phys. Chem.* **1980**, *84*, 178. Scheutjens, J.M.H.M.; Fleer, G.J. *Macromolecules* **1985**, *18*, 1882.
- [19] Scheutjens, J.M.H.M.; Fleer, G.J. in *The Effect of Polymers on Dispersion Properties*; Tadros, Th.F., Ed.; Academic Press: New York, 1982.
- [20] van Male, J., thesis (Wageningen University, 2003).
- [21] Blokhuis, E.M.; Skau, K.I.; Bonet Avalos, J. *J. Chem. Phys.* **119**, 3483 (2003).
- [22] van der Gucht, J.; Besseling, N.A.M.; van Male, J.; Cohen Stuart, M.A. *J. Chem. Phys.* **2000**, *113*, 2886.
- [23] Bolhuis, P.G.; Louis, A.A.; Hansen, J.P.; Meijer, E.J. *J. Chem. Phys.* **2001**, *114*, 4296.

- [24] Fisher, M.E.; Widom, B. *J. Chem. Phys.* **1969**, *50*, 3756.
- [25] Evans, R. *Ber. Bunsenges. Phys. Chem.* **1994**, *98*, 345.
- [26] Silberberg, A. *J. Chem. Phys.* **1968**, *48*, 2835.
- [27] Fleer, G.J.; van Male, J.; Johner, A. *Macromolecules* **1999**, *32*, 825. Fleer, G.J.; van Male, J.; Johner, A. *Macromolecules* **1999**, *32*, 845.
- [28] Daoud, M.; Jannink, G. *J. Phys. (Paris)* **1976**, *37*, 973.
- [29] Skau, K.I., thesis (Leiden University, 2003).
- [30] Ben-Shaul, A.; Szleifer, I.; Gelbart, W.M. *J. Chem. Phys.* **1985**, *83*, 3597. Szleifer, I.; Carignano, M.A. *Adv. Chem. Phys.* **1996**, *94*, 165.
- [31] Bonet Avalos, J.; Mackie, A.D.; Diez-Orrite, S. "Development of an Importance Sampling Single Chain Mean Field Theory for polymer adsorption onto a flat wall", *Macromolecules* (to be published).
- [32] Hanke, A.; Eisenriegler, E.; Dietrich, S. *Phys. Rev. E* **1999**, *59*, 6853.
- [33] Maasen, R.; Eisenriegler, E.; Bringer, A. *J. Chem. Phys.* **2001**, *115*, 5292.
- [34] Whittaker, E.T.; Watson, G.N. *A Course of Modern Analysis*; 4th Ed. Cambridge University Press: Cambridge, 1927.

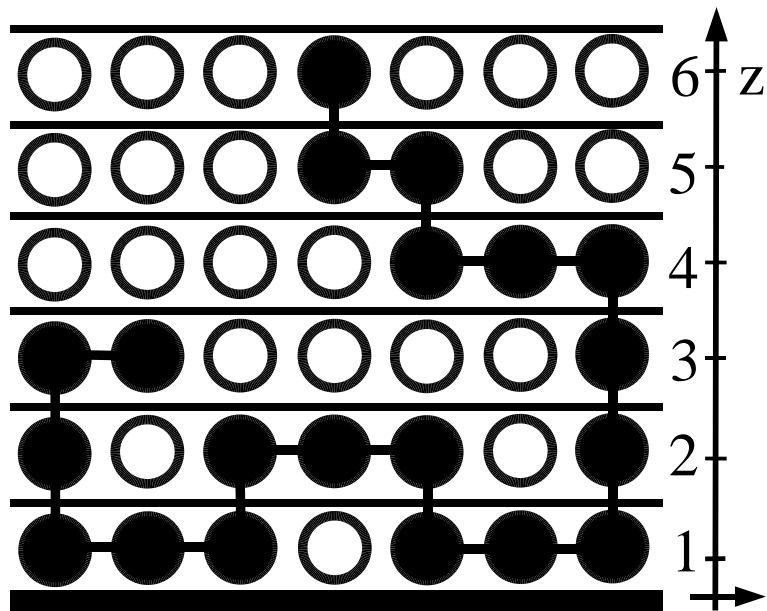
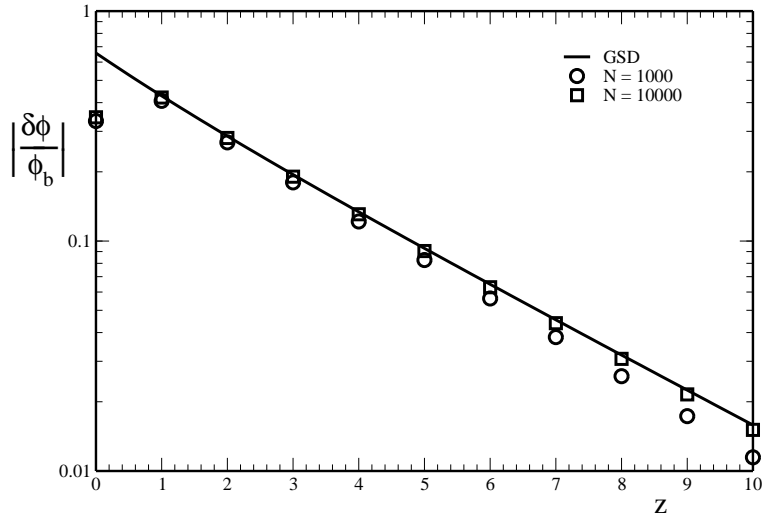
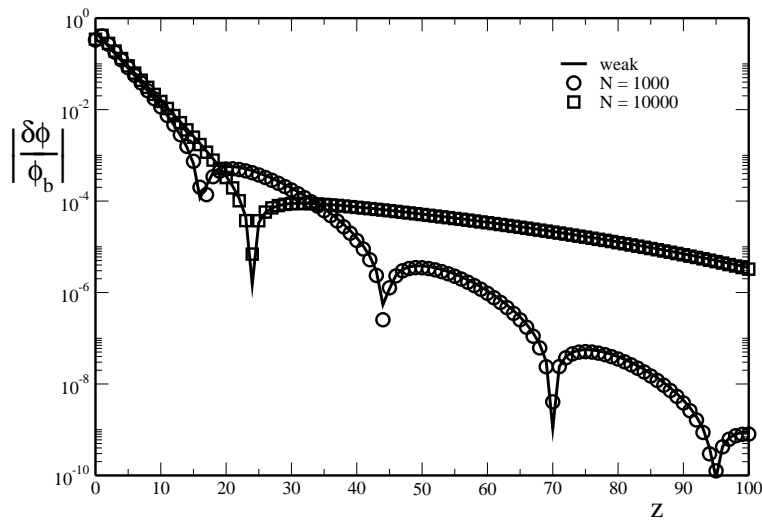


Figure 1: An adsorbed polymer on a lattice. An impenetrable wall is located at $z=0$.



(a)



(b)

Figure 2: Polymer segment density profiles $\delta\phi(z)/\phi_b$ for an athermal solvent ($\chi = 0$) and for $\phi_b = 0.01$. The symbols are the SF calculations for $N = 1000$ (circles) and $N = 10000$ (squares) with $\chi_s = 0.20$. In (a) the solid line corresponds to the de Gennes profile Eq.(4.5). In (b) the solid lines are the density profiles calculated with Eq.(2.17).

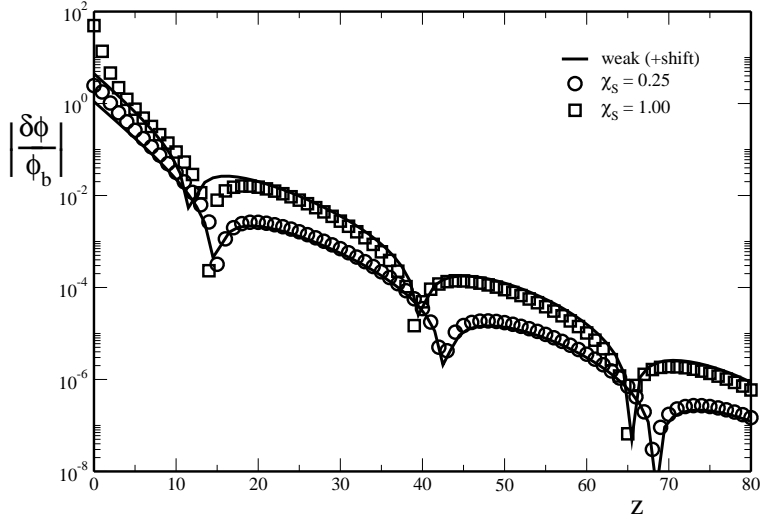


Figure 3: Polymer segment density profiles $\delta\phi(z)/\phi_b$ for an athermal solvent ($\chi = 0$) and for $\phi_b = 0.01$. The symbols are the SF calculations for $\chi_s = 0.25$ (circles) and $\chi_s = 1.0$ (squares) with $N = 1000$. The solid lines are the density profiles calculated with Eq.(2.17) and shifted horizontally by $-1.5a$ (bottom solid line, corresponding to $\chi_s = 0.25$) and $-4.5a$ (top solid line, corresponding to $\chi_s = 1.0$).

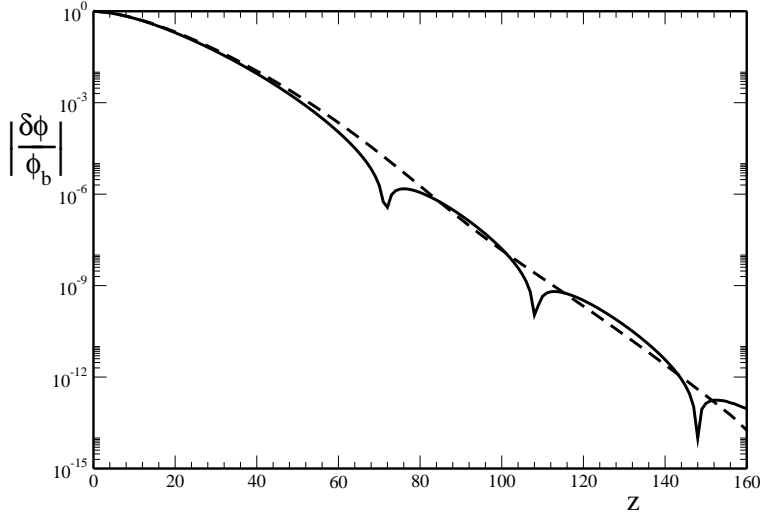
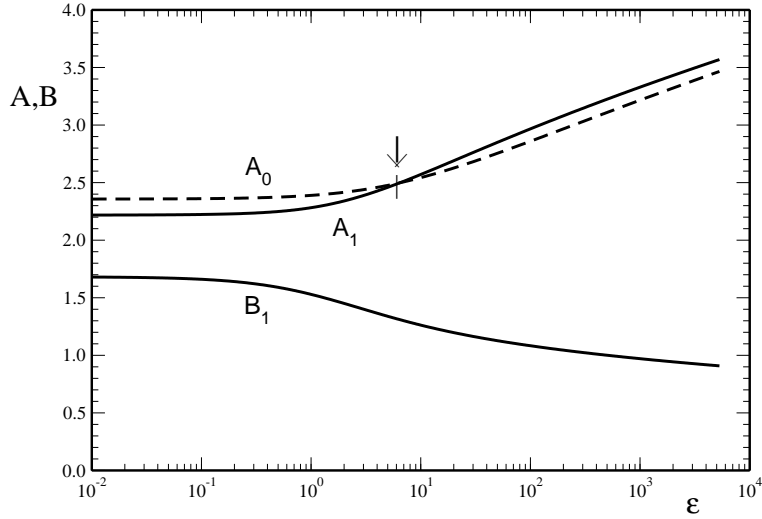
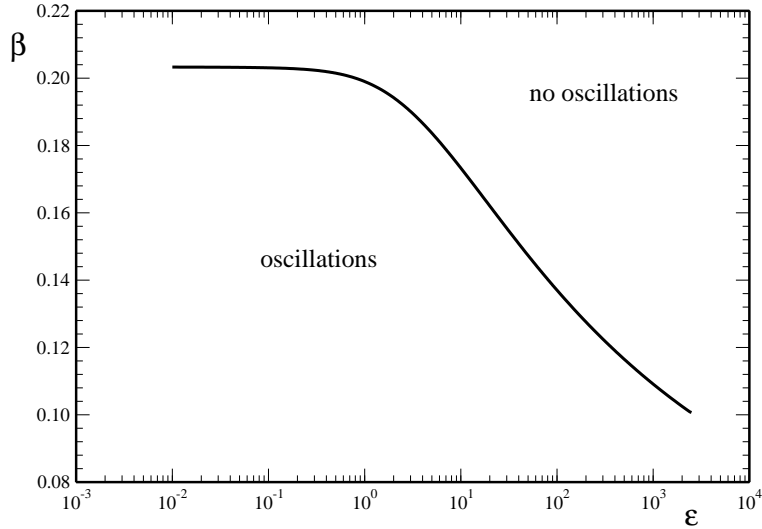


Figure 4: Polymer segment density profiles $\delta\phi(z)/\phi_b$ for a Θ -solvent ($\chi = 0.5$) calculated in the SF model; $\chi_s = -1/12$ and $N = 1000$. The bulk density $\phi_b = 0.01$ (solid line) and $\phi_b = 0.001$ (dashed line).

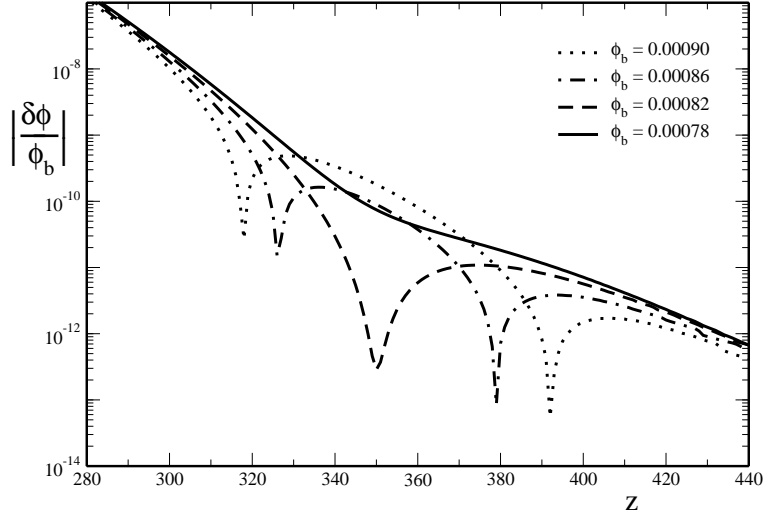


(a)

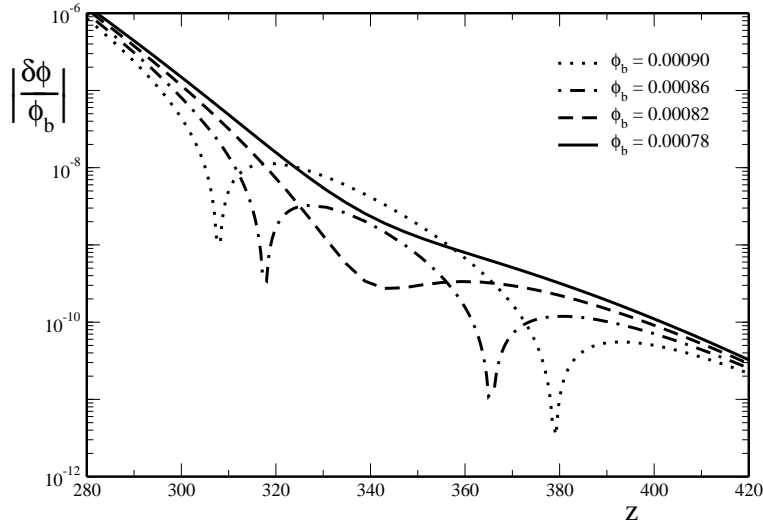


(b)

Figure 5: (a) shows the coefficients A_0 (dashed curve), and A_1 , B_1 (solid curves), that determine the exponential decay and the oscillation period of the polymer density profile (see Eqs.(4.7) and (4.8)), as a function of $\varepsilon = 2/(v\phi_b N)$ for $\beta = 6m/(Na^2v) = 0.18$. At $\varepsilon_{FW} = 6.46398 \dots$, A_0 and A_1 cross. In (b) the locus of Fisher–Widom transitions is shown as a function of ε and β .



(a)



(b)

Figure 6: Polymer segment density profile $\delta\phi(z)/\phi_b$ for a Θ -solvent with $N = 10000$ for various bulk densities: $\phi_b = 0.00078$ (solid line), $\phi_b = 0.00082$ (dashed line), $\phi_b = 0.00086$ (dot-dashed line), and $\phi_b = 0.00090$ (dotted line). In (a), the density profiles are calculated in the SF model, using $\chi_s = -1/12$; in (b) the density profiles are calculated using Eq.(B.6).

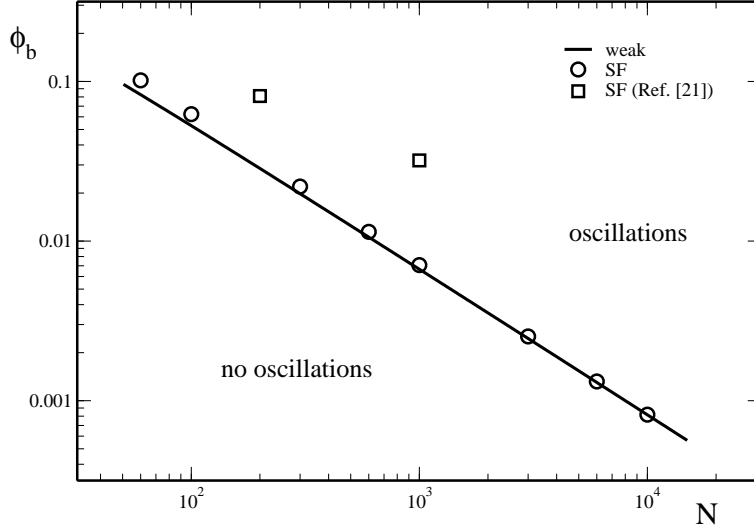


Figure 7: Bulk density corresponding to the Fisher–Widom transition for a Θ -solvent ($\chi = 0.5$) as a function of polymer chain length N . Symbols are the SF calculations for $\chi_s = -1/12$; circles correspond to the present calculations, squares are the results reported in Ref. [22]. The solid line is the analytical result (see text for details).

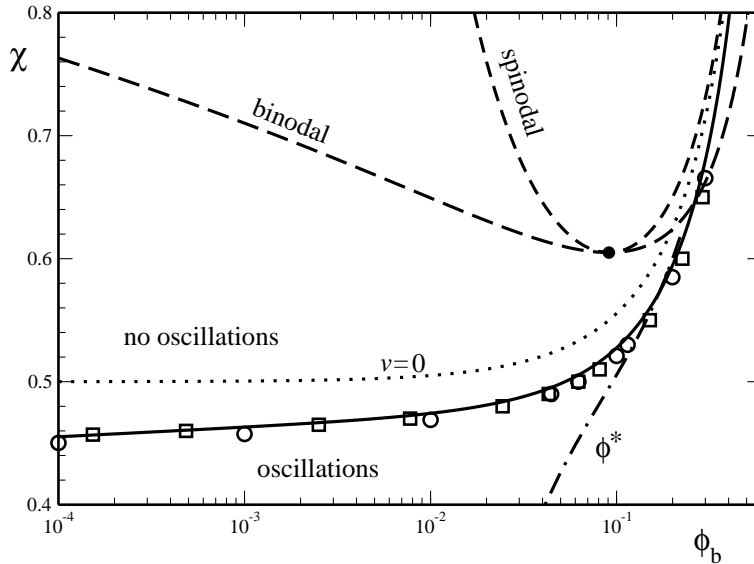
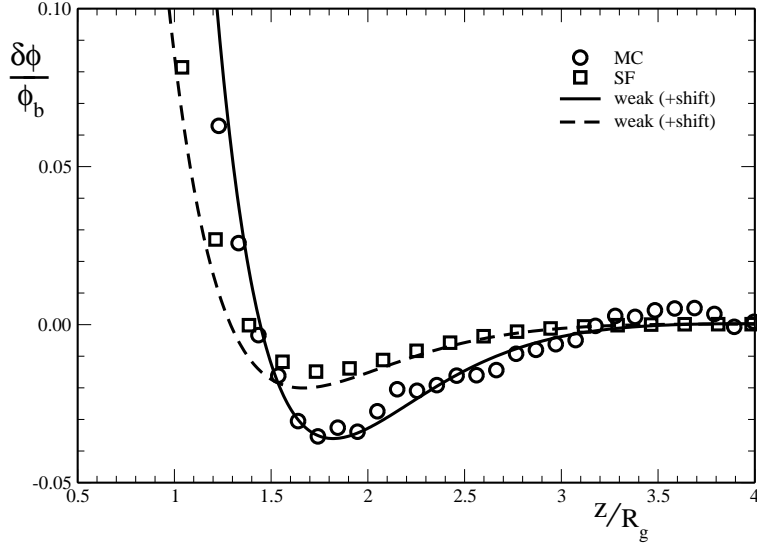
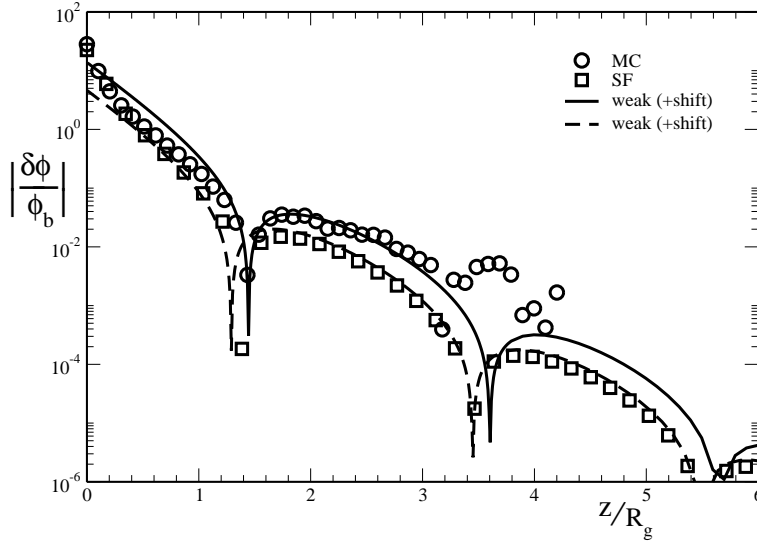


Figure 8: Fisher–Widom transition in the polymer phase diagram for $N = 100$. The symbols are the SF calculations for $\chi_s = 0.5$ (circles) and $\chi_s = 0$ (squares). The solid line is the analytical result (see text for details). The dotted line is where the generalized excluded volume parameter $v = 0$. The dilute to semi-dilute transition is shown as the dot-dashed line ($\phi^* \approx 1/(vN)$). Also shown are the Flory–Huggins spinodal and binodal regions (dashed lines).



(a)



(b)

Figure 9: Reduced polymer segment density profiles ($N = 200$, $\phi_b = 0.0216$). Circles are MC results [15]; squares are the SF calculations for $\chi_s = 1.0$. Solid line is the density profile calculated by Eq.(2.17) for $a/d = 7.35$ and shifted by $-2a$ to fit the MC results. Dashed line is the density profile calculated by Eq.(2.17) for $a/d = 4.09$ (corresponding to $\chi_s = 1.0$) and shifted by $-3.5a$ to fit the SF results. (b) shows the same results on a logarithmic scale.